$(VO)^{2+}$ Ions Immobilized on Functionalized Surface of Mesoporous Silica and Their Activity toward the Hydroxylation of Benzene

Chia-Hung Lee,[†] Tien-Sung Lin,*[,‡] and Chung-Yuan Mou*[,†]

Department of Chemistry, National Taiwan University, Taipei, Taiwan 106, and Department of Chemistry, Washington University, St. Louis, Missouri 63130

Received: August 6, 2002; In Final Form: December 10, 2002

Mesoporous silica MCM-41 was organofunctionalized by 3-aminopropyltrimethoxysilane (APTS) on the surface of its nanochannels. The amino groups of the mesoporous MCM-41 solids were then used to immobilize $(VO)^{2+}$ ions which were employed to study the catalytic oxidation of benzene. We found the vanadium peroxo complex of $V^{5+}-O-O^{\bullet}$ radicals play an important role in the hydroxylation of aromatic hydrocarbons, such as from benzene to phenol. In a series of spectroscopic studies, we found the binding of ligands in these complexes depends on the surface density of APTS, which affects crucially its catalytic activity. The anchored vanadium complexes have better catalytic activities with higher stability than the framework-substituted V−MCM-41 materials. We further demonstrate that immobilization of catalytic metal ion on functionalized surface has the advantages of better control of available reactive sites and site isolation.

Introduction

MCM-41 belongs to a family of mesoporous silicates (M41S) that was invented by Mobil researchers.[1] It has many special characteristics: for instance, high surface area (∼1000 m^2/g), good thermal stability, and hexagonal arrays of uniform 2−10 nm cylindrical pores. Nanopores have been explored as a host for confining various materials and their reactions in recent years, which led to many practical applications, ranging from catalysis,[2,3] to optoelectronics,[4] and to conducting materials.[5] Mesoporous materials now seem to contribute to a wide range of applications, ranging from microelectronics to medical diagnosis.[6] The ability to control the pore size, channel connectivity, morphology, and surface functionality[7] opens up the possibility of using these materials as nanoreactors in which chemical processes can be tailor-designed for detailed studies.

Mesoporous silica materials have been considered as catalyst support.[3,8] Transition metals are often utilized as redox centers. The incorporation of transition metal into the silica frameworks of MCM-41 has been employed to study the catalytic process of liquid-phase oxidation; for instance, the substituted framework of MCM-41 (V−MCM-41) has been synthesized and applied in the oxidization of benzene to phenol in a single step.[9,10] However, the above framework-substituted catalyst suffers from three major disadvantages: (1) low metal content, (2) decaying catalytic activities where metal is easily leached from the framework during and after the catalytic reaction, and (3) poor control of the molecular environment of the catalytic site. Our objective is to design well-defined catalytic sites on the surface of mesoporous materials that could minimize the above disadvantages. In other words, our goal is to acquire the flexibility of controlling ligands on the catalytic center while immobilizing the catalyst at the same time.

Research on immobilization of homogeneous catalysts has received a lot of attention recently.[11] Previously, 3-aminopropyltrimethoxysilane (APTS) was used to organofunctionalize MCM-41 and to coordinate Fe^{3+} and Cu^{2+} ions to provide active metal catalysts ($MCM41-NH_2-M$ with M = Fe or Cu).[12] They demonstrated these immobilized metal catalysts can affect the oxidation of cyclohexane with H_2O_2 in the liquid phase. The same approach was also employed to graft Mn^{2+}, Cu^{2+}, Co^{2+}, and Zn^{2+} ions onto the surface of H_1SiO_2 (a mesoporous material using a nonionic surfactant as a template) channels. These catalysts have been shown to be effective in the redox reactions of *o*-aminophenol, *o*-phenylenediamine, and *p*-phenylenediamine. Even though some analyses of the kinetics and mechanism of these redox reactions have been described previously,[13] the chemical environments of the metal centers in these catalysts have not yet been clearly elucidated in these studies.

In this paper, we shall show the immobilization of metal catalyst in the mesoporous channels provides us with a good opportunity to control its chemical environment and thus catalytic activity. We first functionalize the surfaces of MCM-41 and silica gel with amino groups and then incorporate $(VO)^{2+}$ ions to form an extraframework vanadium oxide catalyst on the channel surface. We carefully characterize the chemical environment of the vanadium centers in $MCM41-NH_2-(VO)$ and silica $gel-NH_2-(VO)$ solids by various spectroscopic techniques.

We shall demonstrate that $(VO)^{2+}$ ions form strong coordination by covalent bonding with multiple amino groups. The grafted vanadium metals show good stability and do not seriously leach from the $MCM41-NH_2-(VO)$ solids during the catalytic process. We shall further demonstrate the catalytic activities of these extraframework catalysts are better than that of the framework-substituted V−MCM-41, specifically for the preparation of phenols. Conventionally, phenols have been prepared by the Hock process, where cumene is oxidized to cumene hydroperoxide in the air and in aqueous emulsion (Na_2CO_3) and subsequent cleaved in acidic media.[14] This is a complicated multiple-step process with acetone as a byproduct.

* To whom correspondence should be addressed. E-mail: lin@wuchem.wustl.edu (T.-S.L.); cymou@ms.cc.ntu.edu.tw (C.-Y.M.).
[†] National Taiwan University.
[‡] Washington University.

10.1021/jp026703f CCC: $25.00
Published on Web 02/21/2003

SCHEME 1

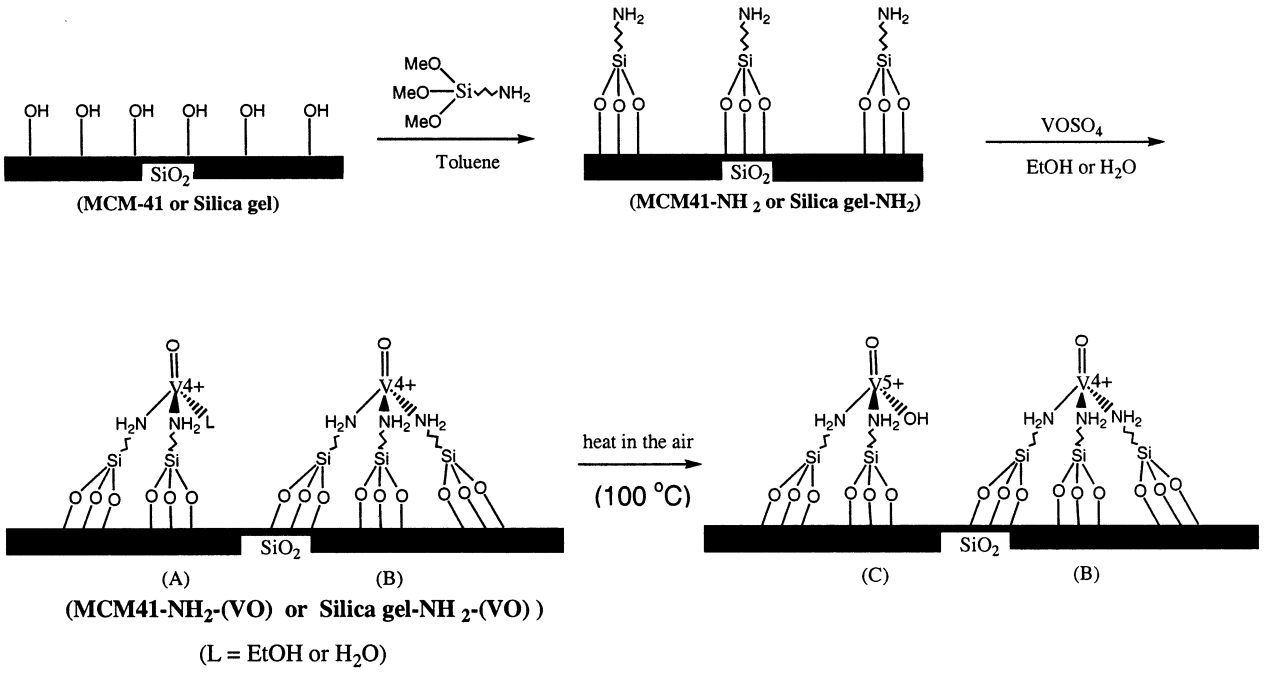

We are therefore motivated to develop a high-yield one-step process.

Experimental Section

1. Preparation of Catalysts. *(a) Synthesis of MCM-41.* MCM-41 was prepared according to a recipe given previously.[15] Briefly, 27.4 g of cetyltrimethylammonium bromide (CTAB) was fully dissolved in 240 g of water. A portion of 35.6 g of sodium silicate solution was added to the above mixture under stirring. A sample of 42 g of 1.2 M H_2SO_4 was added slowly to the resulting mixture by pipet under stirring for 1 h at 32 °C and then hydrothermalized at 100 °C for 2 days in a PTFE-lined autoclave. The final product was recovered by filtration, followed by washing twice with deionized water, dried at 100 °C, and calcined at 540 °C for 8 h.

(b) Silylation of MCM-41 and Silica Gel: Preparation of MCM41−NH_2 or Silica Gel−NH_2 Solids (Scheme 1). The anchoring of 3-aminopropylsilyl groups onto MCM-41 and silica gel were prepared as follows: 0.5 g of the calcined MCM-41 or silica gel was placed in 100 mL of toluene and stirred for 30 min. A sample of 2.5 g of APTS was added to the resulting mixture. The above reaction was allowed to run overnight at 110 °C. The solids were washed twice with toluene and acetone. The filtered sample was dried under vacuum.

(c) Complexation of $(VO)^{2+}$ Ions in MCM41−NH_2 or Silica Gel−NH_2 Solids (Scheme 1). (i) In alcohol solution, 1 g of MCM41−NH_2 or silica gel−NH_2 was introduced into a saturated $VOSO_4$−EtOH solution, stirred for 20 min, then filtered, and washed with pure alcohol. The final solids were added to a fresh $VOSO_4$−EtOH solution. This step was repeated three times to achieve the maximal $(VO)^{2+}$ ions coordinated to the amino groups on the surface. The sample was filtered and dried under vacuum to obtain the MCM41−NH_2−(VO)−EtOH solids or the corresponding silica gel solids.

(ii) In water solution, 0.32 g of $VOSO_4$ was dissolved in 20 mL of deionized water and 1 g of MCM41−NH_2 or silica gel−NH_2 solid under stirring for 20 min. The solids were recovered by filtration, followed by washing with deionized water, and then added to a fresh $VOSO_4$−H_2O solution. We repeated this step three times to ensure the saturated $(VO)^{2+}$ ions coordinated to the amino groups on the surface. The filtered sample was dried under vacuum to obtain the MCM41−NH_2−(VO)−H_2O solids or the corresponding silica gel solids.

(d) Synthesis of V−MCM-41. The preparation of framework-substituted V−MCM-41 in alkali condition has been described previously.[10] Briefly, 1.37 g of CTAB was fully dissolved in 10 g of water and stirred until a clear solution was obtained. Then, 0.1 g of $VOSO_4$ in 1 mL of H_2O solution was added to the surfactant solution under stirring. Samples of 1.77 g of sodium silicate and 1.7 g of 1.2 M H_2SO_4 were added slowly to the resulting mixture by pipet under stirring for 2 h at 32 °C. The resultant product was washed thoroughly with water. The sample was dried at 100 °C and calcined at 540 °C for 8 h.

2. Spectroscopic Characterization of Catalysts. The structures of these catalysts were analyzed by X-ray powder diffraction (XRD) (Scintag X1 diffractometer, Cu Kα radiation at $\lambda = 0.154$ nm). The surface area and pore size was determined by N_2 adsorption−desorption isotherms obtained at 77 K on a Micrometric ASAP 2010 apparatus. The sample was outgassed at 10^{-3} Torr and 300 °C for about 6 h prior to the adsorption experiment. The pore size distribution curves were obtained from the analysis of the desorption portion of the isotherms using the BJH (Barrett−Joyner−Halenda) method.

FTIR spectra were recorded on a Nicolet 550 spectrometer using a KBr pellet. About 1 mg of sample was mixed with 300 mg of dried KBr and then pressed. The diffuse reflectance UV−vis spectra were measured with a Shimadzu UV-2101PC. Powdered samples were loaded in a quartz cell, and spectra were collected in the 200−800 nm wavelength range against a standard.

EPR spectra were recorded on an X-band EPR spectrometer (Bruker ER300). A flat rectangular quartz sample cell was used to measure the EPR spectra of liquid mixtures. A quartz tubing of 4 mm o.d. was used to measure the EPR spectra of solids. The spectrometer was equipped with a variable-temperature setup, which allowed us to perform low-temperature experiments (100 K to room temperature) of solids. A sample of DPPH

SCHEME 2

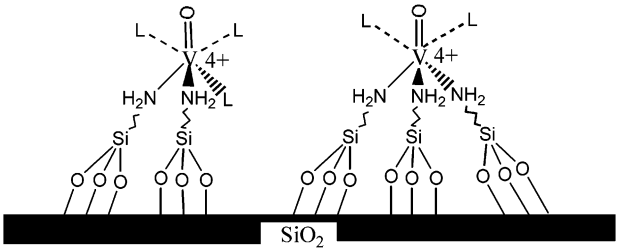

Coordination $(VO)^{2+}$ in H_2O-$VOSO_4$ solution : L=H_2O.
Coordination $(VO)^{2+}$ in D_2O-$VOSO_4$ solution : L=D_2O.
Coordination $(VO)^{2+}$ in EtOH-$VOSO_4$ solution : L=EtOH.

($g = 2.0036$) was used as the reference sample for the *g*-value determination.

3. Measurements of Catalytic Activity. *(a) Generation and Detection of Hydroxyl Radicals.* Hydroxyl radicals (•OH) were generated via the Fenton-like reaction ($V^{4+} + H_2O_2$) (see Scheme 3). Since •OH radicals are short-lived species, we employed a spin-trapping agent DMPO (5,5-dimethyl-1-pyrroline *N*-oxide) to trap and convert the reactive radicals to stable nitroxides, •DMPO−OH. The composition of a typical mixture of reagents used in the experiment was 3 mg of MCM41−NH_2−(VO) or silica gel−NH_2−(VO) solids, 50 μL of 0.1 M DMPO, 50 μL of 0.1 M H_2O_2, and 400 μL of H_2O. The mixture was vigorously shaken for 10 s, and the liquid was extracted by means of syringe filters. The EPR spectra of the liquid were taken 3 min after the mixing.

(b) Generation and Detection of Dioxygen Radicals. Dioxygen radicals were generated via V^{4+} in excess H_2O_2 (see Scheme 3). The composition of a typical mixture of reagents used in the experiment was 25 mg of MCM41−NH_2−(VO) or silica gel−NH_2−(VO) solids and 200 μL of 3.2 M H_2O_2 in CH_3CN. The mixture was vigorously shaken for 10 s, and the solids were separated from the liquid by means of syringe filters. The EPR spectra of the solids were taken 2 min after the mixing.

(c) Hydroxylation of Benzene. The catalyst was first placed in a 50 mL round-bottom flask with a condenser cooled at 5 °C, and then benzene and CH_3CN were added. After stirring for 10 min, the oxidant was added dropwise and the reaction temperature was maintained at 60 °C. The reaction conditions are as follows:

(i) H_2O_2 as the oxidant: 100 mg of catalyst, 10 mmol of benzene, 10 mmol of H_2O_2 (35%), 6 mL of CH_3CN, and reaction time 1 h.

(ii) TBHP (*tert*-butyl hydroperoxide) as the oxidant: 100 mg of catalyst, 10 mmol of benzene, 10 mmol of TBHP (70%), 6 mL of CH_3CN, and reaction time 6 h.

The products were analyzed by a Gilson 306 liquid chromatograph using an RP Amide C_{16} (4.6 × 250 mm) column, acetonitrile and water as a mobile phase (acetonitrile: water = 70:30), and a UV−vis detector at 260 nm wavelength.

Results and Discussion

1. Physical Properties. *(a) Surface Area and Pore Diameters of Mesoporous Materials.* The surface areas and pore diameters are given in Table 1. We note that the surface area is reduced from 1102 m^2/g in the unmodified MCM-41 to 690 m^2/g in the modified MCM41−NH_2, a 30% reduction. After the $-O_3Si(CH_2)_3NH_2$ modification, the pore diameter of the mesoporous material is also reduced from 2.57 to 1.94 nm. The reduction in the surface area and pore diameter indicates the $-O_3Si(CH_2)_3NH_2$ groups are attached on the inner wall surface of the nanochannels. When $(VO)^{2+}$ ions are coordinated on the surface of MCM41−NH_2, we observe a further 40% reduction of the surface area. Since the $(VO)^{2+}$ ions are well dispersed inside the channel pores, some fraction of the surface area of the channel is now occupied by the metal complexes. We also observe the reduction of surface area in the coordination of $(VO)^{2+}$ ions in silica gel−NH_2 solids.

(b) Elemental Analysis. The data of elemental analysis are also given in Table 1. A simple calculation shows there is 1.85 mmol of $-O_3Si(CH_2)_3NH_2$ per gram of MCM41−NH_2 solids and 1.92 mmol of $-O_3Si(CH_2)_3NH_2$ per gram of silica gel−NH_2 solids. The density of amino groups in MCM-41 is 1.62 (number of $-O_3Si(CH_2)_3NH_2/(nm)^2$), and that in silica gel is 3.95 units. We further used ICP−AES to determine the amount of vanadium metal in the catalysts; we found there is 24 ± 4 mg of vanadium per gram of MCM41−NH_2 and silica gel−NH_2 sample. The mole ratios of nitrogen to vanadium metal ($-O_3Si(CH_2)_3NH_2$:vanadium) of these samples can be further

SCHEME 3

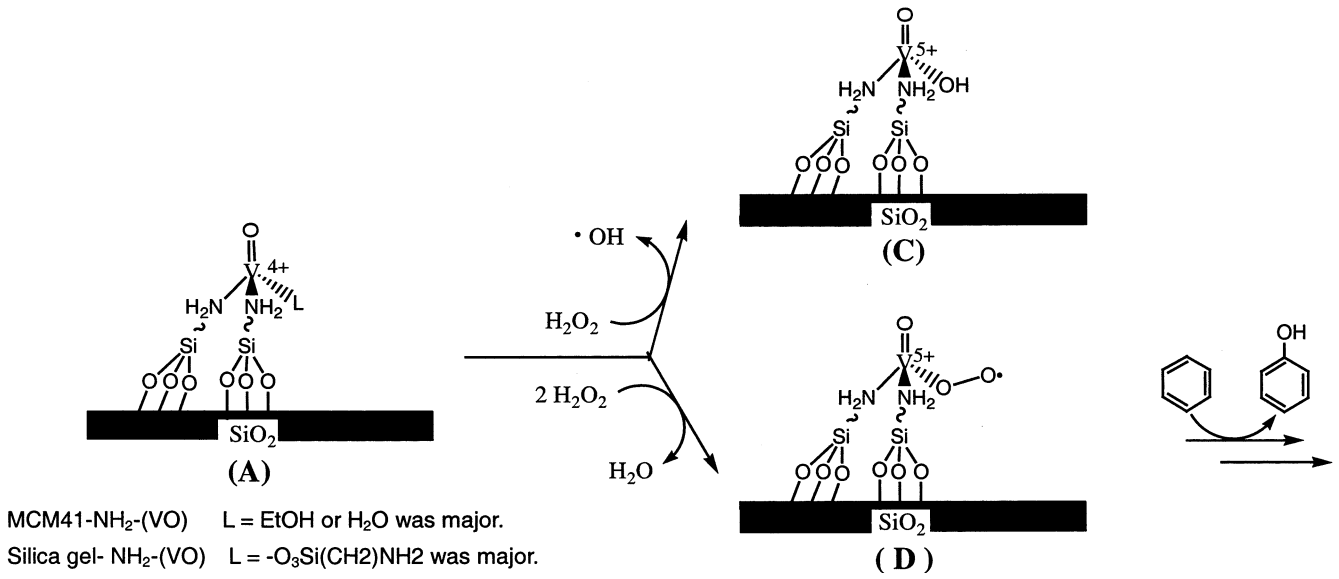

MCM41-NH_2-(VO) L = EtOH or H_2O was major.
Silica gel- NH_2-(VO) L = -O_3Si(CH2)NH2 was major.

TABLE 1: Surface Area, Pore Diameter, Density of Amino Groups, and Vanadium Content

sample	surf. area, m^2/g	pore diam, nm	density of amino groups, no. of $-O_3Si(CH_2)_3NH_2/(nm)^2$	V content, mg of V/g of catalyst
MCM-41	1102	2.57	ND[a]	ND
V−MCM-41	1090	2.69	ND	20.7
MCM41−NH_2	690	1.94	1.62	ND
MCM41−NH_2–(VO)−H_2O	334	1.87	2.18	25.7
MCM41−NH_2–(VO)−EtOH	393	1.99	2.10	28.4
silica gel	442	ND	ND	ND
silica gel−NH_2	293	ND	3.95	ND
silica gel−NH_2–(VO)−H_2O	200	ND	4.31	26.6
silica gel−NH_2–(VO)−EtOH	212	ND	3.57	20.7

[a] ND: not determined.

TABLE 2: Structural Differences of MCM41−NH_2−(VO)−L and Silica Gel−NH_2−(VO)−L

sample	$-O_3Si(CH_2)_3NH_2$/V mole ratio	complex **A**:complex **B** mole ratio[a]
MCM41−NH_2–(VO)−H_2O	2.40 ± 0.02	60 (L = H_2O):40
MCM41−NH_2–(VO)−EtOH	2.46 ± 0.01	54 (L = EtOH):46
silica gel−NH_2–(VO)−H_2O	2.74 ± 0.03	26 (L = H_2O):74
silica gel−NH_2–(VO)−EtOH	3.09 ± 0.01	0 (L = EtOH):100

[a] Complex **A** has two $-O_3Si(CH_2)_3NH_2$ groups attached to $(V{=}O)^{2+}$, and complex **B** has three units (see Scheme 1).

calculated and are given in Table 2. The mole ratio of N:V in MCM41−NH_2−(VO)−H_2O sample is 2.40, and that in MCM41−NH_2−(VO)−EtOH sample is 2.46. The mole ratios indicate that MCM41−NH_2−(VO) samples may have two (designated as complex **A**, see Scheme 1) or three (complex **B**) $-O_3Si(CH_2)_3NH_2$ groups coordinating on one $(VO)^{2+}$ ion. Moreover, in the case of the silica gel−NH_2−(VO) sample, the mole ratio of N:V in silica gel−NH_2−(VO)−H_2O is 2.74, and that in silica gel−NH_2−(VO)−EtOH is 3.09. These ratios indicate there are more $-O_3Si(CH_2)_3NH_2$ groups coordinating on the $(VO)^{2+}$ ion in the silica gel−NH_2−(VO) than that in the MCM41−NH_2−(VO) samples.

The ratios of complex **A**:complex **B** for different samples are also given in Table 2. The results indicate that MCM41−NH_2−(VO) samples have higher amounts of complex **A** than silica gel−NH_2−(VO) samples. We shall further demonstrate that different ratios of complex **A** and complex **B** in MCM-41 and silica gel will have different catalytic activities (see below).

2. Spectral Characterization. *(a) X-ray Diffraction Pattern.* The XRD pattern of MCM41−NH_2 solids is shown in Figure 1a. The pattern consists of four Bragg reflexes which can be indexed in a hexagonal symmetry with *hkl* triplets of (100), (110), (200), and (210).[1,16] The presence of these four Bragg reflexes indicates that the catalyst possesses a highly ordered structure. The 2θ values of the d_{100} peaks remain the same except for the decrease in intensity after the $(VO)^{2+}$ ions are grafted onto the MCM41−NH_2 solids in EtOH−$VOSO_4$ solution (Figure 1b) or H_2O−$VOSO_4$ solution (Figure 1c). The decrease in the intensity of the (100) peak may be attributed to some extent of structural collapse in the ordered hexagonal phase, or the flexibility of the silica framework resulting from the strain of the incorporated metal complex.

To further examine the possibility of structural changes, we plot the derivative of the pore volume per unit weight against the pore diameter (d*V*/d*D*), which is shown in the inset of Figure 1. After the $(VO)^{2+}$ ions are grafted onto the MCM41−NH_2 solids, the pore size remains about the same but the distribution becomes narrower and sharper, which implies the structure of mesoporous solid remains unaffected, and the $(VO)^{2+}$ ions are more uniformly dispersed inside the channel pores.

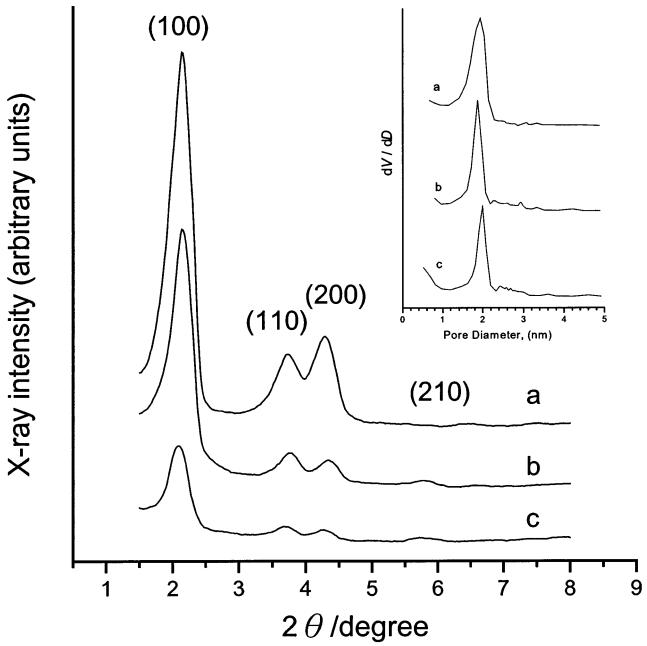

Figure 1. X-ray powder diffraction patterns of (a) MCM41−NH_2, (b) MCM41−NH_2−(VO)−EtOH, and (c) MCM41−NH_2−(VO)−H_2O. The inset shows the plot of the derivative of the pore volume per unit weight against the pore diameter (d*V*/d*D*).

(b) FTIR Spectra. Figure 2a shows the IR spectra in the 500−4000 cm^{-1} region of MCM-41 solids. The MCM41−NH_2 sample displays the N−H bending mode (primary amine) at 1546 cm^{-1} and C−H stretching at 2944 cm^{-1} (Figure 2b), which indicate the presence of $-Si(CH_2)_3NH_2$ on the wall surface. After coordinating $(VO)^{2+}$ ions on the surface of MCM41−NH_2 solids, the original N−H bending (primary amine) at 1546 cm^{-1} is shifted to 1513 cm^{-1} (Figure 2c). The IR spectra indicate most of the amino groups are coordinated with $(VO)^{2+}$ ions.

(c) Diffuse Reflectance UV−Visible Spectra. After heating the solids in air at 100 °C for 24 h, the UV−vis spectrum of the coordinated $(VO)^{2+}$ ions on MCM41−NH_2 surface in the H_2O−$VOSO_4$ solution is taken and displayed in Figure 3a. The spectrum of MCM41−NH_2−(VO)−H_2O solids shows two intense absorption bands at 220 nm and a broad shoulder at 340 nm. The asymmetric line shape of the intense 220 nm band indicates a weak band at ∼280 nm hidden beneath the strong band as evidenced in the following analysis. The absorption band at 220 nm has been attributed to the silica materials,[9] such as MCM-48.[17] On the other hand, the absorption bands at ca. 280 and 340 nm have been assigned to the low-energy charge transfer (CT) bands between V=O electron transfer $(\pi)t_2 \rightarrow$ (d)e and $(\pi)t_1 \rightarrow$ (d)e of tetrahedrally coordinated V^{5+} ions.[18,19]

We further observed a weak broad absorption at 600−800 nm which may be assigned to the d−d transition of $(VO)^{2+}$

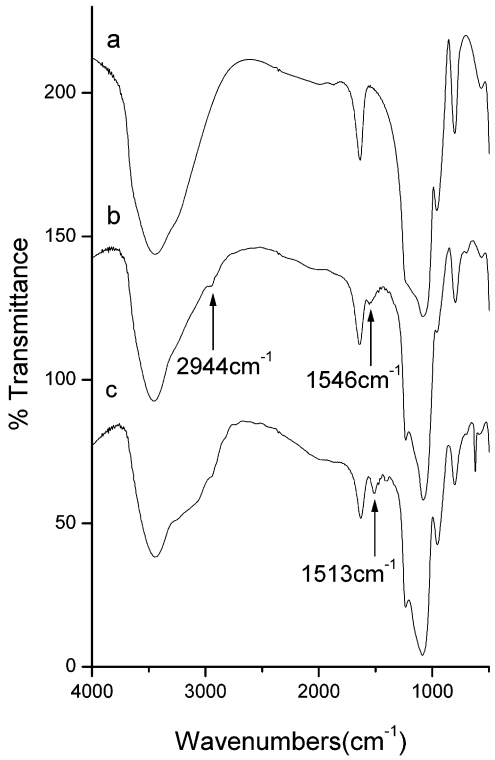

Figure 2. FTIR spectra of (a) MCM-41, (b) MCM41−NH_2, and (c) MCM41−NH_2−(VO)−H_2O solids.

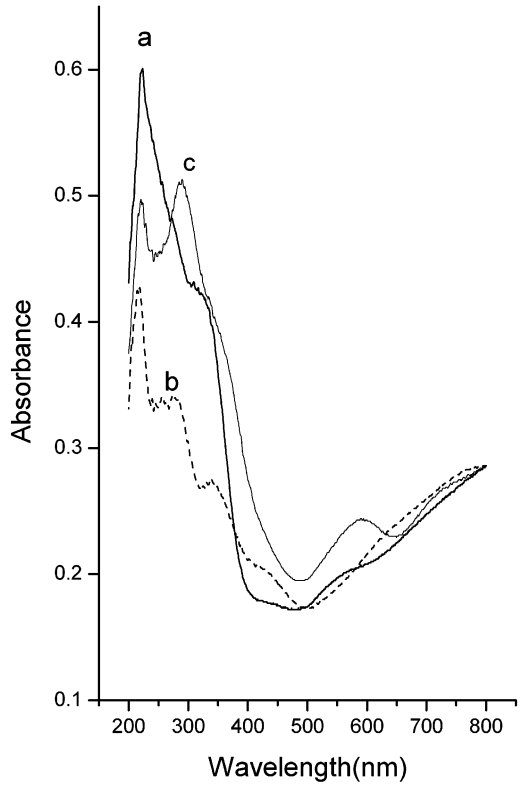

Figure 3. Diffuse reflectance UV−vis spectra of the following solids: (a) MCM41−NH_2−(VO)−H_2O (after heating in air at 100 °C for 24 h), (b) MCM41−NH_2−(VO)−EtOH, and (c) MCM41−NH_2−(VO)−EtOH (after heating in air at 100 °C for 24 h).

cation.[20] Since the d−d transitions are generally 10−30 times lower than those of CT transitions, it may account for the low intensity observed at 600−800 nm in comparison to the bands at 280 or 340 nm. On the basis of the appearance of green color

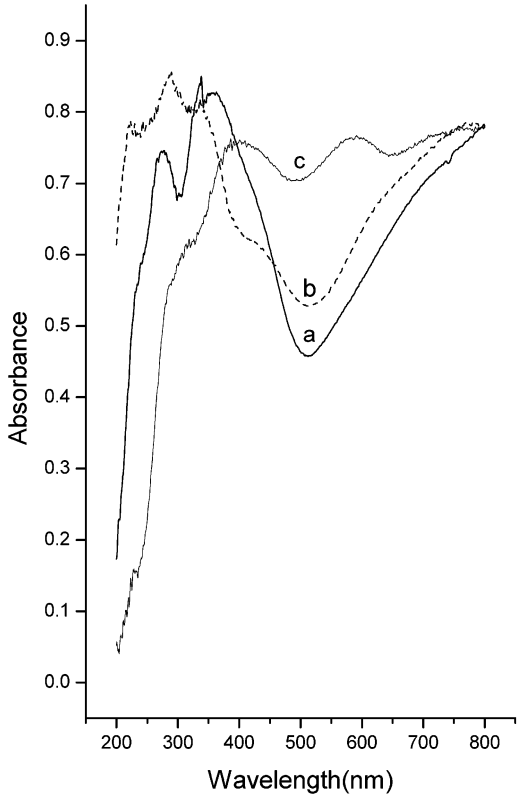

Figure 4. Diffuse reflectance UV−vis spectra of the following solids: (a) silica gel−NH_2−(VO)−H_2O (after heating in air at 100 °C for 24 h), (b) silica gel−NH_2−(VO)−EtOH, and (c) silca gel−NH_2−(VO)−EtOH (after heating in air at 100 °C for 24 h).

of the sample, weak absorption band in the long wavelength, and the EPR study of these samples (see below), the sample should contain a mixture of $(VO)^{2+}$ and V^{5+}.

When $(VO)^{2+}$ ions are coordinated on MCM41−NH_2 surface in the EtOH−$VOSO_4$ solution, we observed these absorptions at 220, 280, 340, and 600−800 nm (Figure 3b). Here the 280 nm band is clearly resolved in the EtOH solvent. However, after heating of the solids in air at 100 °C overnight, the intensities of both 280 and 340 nm bands increase, and the intensities at 600−800 nm decrease (Figure 3c). The change of intensity indicates some of V^{4+} ions were oxidized to V^{5+} complexes upon heating. In addition, a new absorption band appears around 580 nm which has been assigned to an octahedral V^{5+} species (moist air may provide the extra H_2O ligand).[18]

Figure 4 displays the diffuse reflectance UV−vis spectrum of silica gel−NH_2−(VO) solids. The spectrum of the coordination of $(VO)^{2+}$ ions on silica gel−NH_2 surface in H_2O−$VOSO_4$ solution and heated in air at 100 °C is shown in Figure 4a. This spectrum of silica gel−NH_2−(VO)−H_2O also exhibits UV−vis absorption bands at 220, 280, 340, and 600−800 nm. In general, the absorption intensities of silica gel−NH_2−(VO) solids are greater than those of MCM41−NH_2−(VO), especially the absorption intensity at 600−800 nm. This may arise from higher density of amino group coordinating to $(VO)^{2+}$ ions (see Table 2), which could restrain V^{4+} from further oxidation.

The spectrum for the silica gel−NH_2 coordinated $(VO)^{2+}$ ions in EtOH−$VOSO_4$ solution is displayed in Figure 4b. The spectrum for the sample dried in air at 100 °C is shown in Figure 4c. We observed two new absorption bands at 415 and 550 nm in Figure 4c. We assign the band at 415 nm to the CT transition of the V═O double bond of square pyramidal V^{5+} ions,[17,18,21] and that at 550 nm to the CT transition of octahedral V^{5+} species.[18]

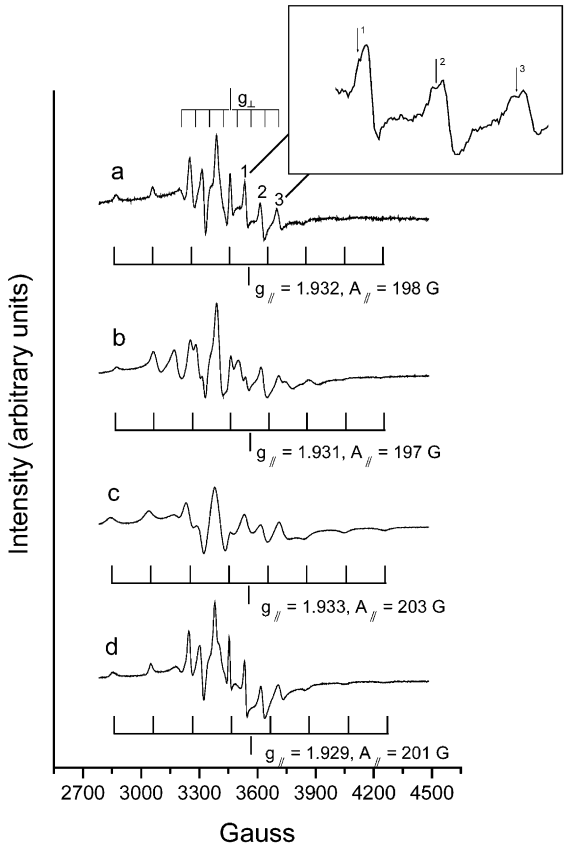

Figure 5. EPR spectra of (a) MCM41−NH_2−(VO)−H_2O, (b) MCM41−NH_2−(VO)−D_2O, (c) MCM41−NH_2−(VO)−EtOH, and (d) MCM41−NH_2−(VO)−EtOH solids after heating in air at 100 °C for 24 h. The inset shows each of the spectral lines is further split into two, which are assigned to two different complex configurations.

(d) EPR Measurements. The EPR spectra of MCM41−NH_2−(VO) and silica gel−NH_2−(VO) samples are shown in Figures 5 and 6. All samples exhibit a typical V^{4+} ($3d^1$) center with characteristic eight-line hyperfine patterns due to the interaction of an unpaired electron with nuclear spin $I = 7/2$ of ^{51}V (natural abundance 99.8%). The well-resolved hyperfine patterns further indicate that the paramagnetic center $(VO)^{2+}$ is well dispersed in the sample. The $g_{||}$ values of these samples are very similar to each other (1.932 ± 0.003). It has been reported that the most common coordination of vanadium is octahedral or square pyramidal often with tetragonal distortions.[21] Our observed g values and hyperfine coupling constants are similar to the values reported for $(VO)^{2+}$ complexes in MCM-41 framework in a square pyramidal coordination, but these spectral parameters are also similar to those of the $(VO)^{2+}$ ions in VS-1 and ZSM-5 solids in distorted octahedral site symmetry.[22,23] However, they are very different from those reported for $(VO)^{2+}$ in tetrahedral coordination.[24] On the basis of the structural consideration as proposed in Scheme 2, we assign $(VO)^{2+}$ ions to the distorted octahedral coordination. The extra ligands may come from the solvent molecules, which can yield the distorted octahedral complex.

Figure 5a shows the EPR spectrum of $(VO)^{2+}$ ions coordinating to the surface of MCM41−NH_2 sample in H_2O−$VOSO_4$ solution. The paramagnetic parameters are $g_{||} = 1.932 \pm 0.001$ and $A_{||} = 198 \pm 2$ G, where A is the hyperfine coupling constant. The perpendicular component has the following parameters: $g_{\perp} = 1.985 \pm 0.002$ and $A_{\perp} = 70 \pm 3$ G. We further observe that each of the spectral lines of the perpendicular components is barely split into two lines (see inset), which indicates the presence of two species. We assign them to complexes **I** and **II** (L = H_2O) (**I** and **II** designation are arbitrary, see Scheme 2).

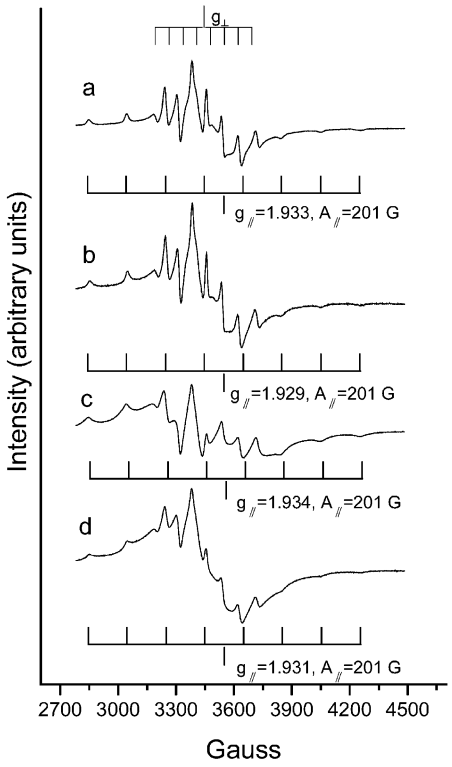

Figure 6. EPR spectra of (a) silica gel−NH_2−(VO)−H_2O, (b) silica gel−NH_2−(VO)−D_2O, (c) silica gel−NH_2−(VO)−EtOH, and (d) silica gel−NH_2−(VO)−EtOH solids after heating in air at 100 °C for 24 h.

To confirm our assignment, we prepared the coordinating complexes in D_2O−$VOSO_4$ solution. The EPR spectrum of the deuterated sample is shown in Figure 5b. The parameters of complexes are $g_{||} = 1.931$ and $A_{||} = 197$ G. The splittings of spectral lines in the perpendicular components are more pronounced in the deuterated sample. Again we assign them to complexes **I** and **II** (L = D_2O).

Figure 5c shows the EPR spectrum of $(VO)^{2+}$ ions coordinating on MCM41−NH_2 surface in EtOH−$VOSO_4$ solution. The spectrum is relatively broad, which may result from the overlapping of two similar environments of complexes **I** and **II** (L = EtOH). The parameters are $g_{||} = 1.933$ and $A_{||} = 203$ G. If the sample was heated in the air at 100 °C for 24 h, the spectrum became sharper as shown in Figure 5d. The spectral change may arise from the oxidation of complex **I** (L = EtOH) to complex **C** (see Scheme 1). Since the V^{5+} (d^0) is EPR silent, the signal at $g_{||} = 1.929$ and $A_{||} = 201$ G should belong to complex **II**.

Figure 6 shows the EPR spectra of $(VO)^{2+}$ ions coordinated in silica gel−NH_2 solids: (a) H_2O−$VOSO_4$, (b) D_2O−$VOSO_4$, (c) EtOH−$VOSO_4$ (before heating), and (d) EtOH−$VOSO_4$ (after heating) in air at 100 °C for 24 h. The paramagnetic parameters of all these samples are about the same: $g_{||} = 1.932 \pm 0.003$ and $A_{||} = 201 \pm 2$ G. The results indicate they are in the same environment. In addition, we do not observe any spectral splitting in Figure 6a,b. Therefore, the major component in Figure 6a,b should be complex **II**.

Figure 6d shows the spectrum for the preheated sample of silica gel−NH_2−(VO)−EtOH, which is almost the same as Figure 6c except a broadening in the central region that may imply the presence of some isolated $(VO)^{2+}$ions. The EPR

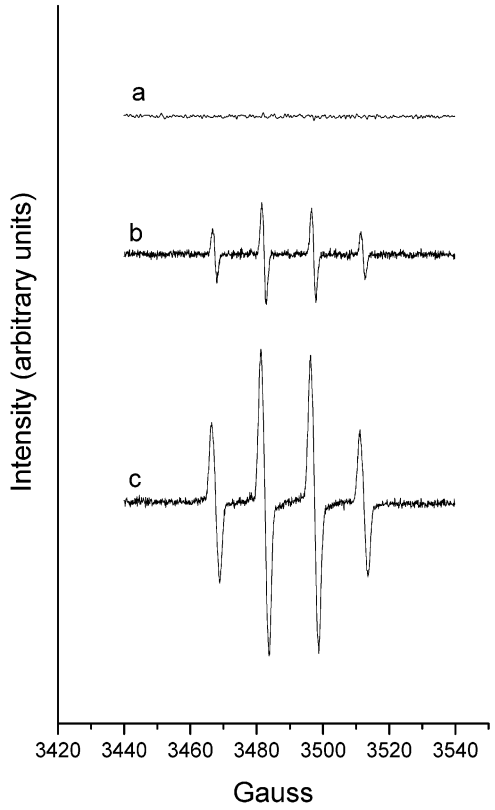

Figure 7. Spin trapping/EPR spectra of •DMPO−OH radical intensity (liquid phase at room temperature) arising from different solids reacted with H_2O_2: (a) V−MCM-41 after calcinations at 560 °C, zero intensity indicates all of the V^{4+} being converted to V^{5+}; (b) MCM41−NH_2−(VO)−H_2O; and (c) silica gel−NH_2−(VO)−H_2O samples. We note that the intensity of •DMPO−OH radicals is proportional to the amount of V^{4+} available for the oxidation reaction of H_2O_2.

spectral results indicate that complex **II** is the major component in the silica gel samples. Note that complex **II** contains three units of $-O_3Si(CH_2)_3NH_2$ and is less vulnerable for oxidation.

3. Catalytic Activities. *(a) Generation of •OH Radicals.* Hydroxyl radicals were generated via the following Fenton-like reaction and trapped by DMPO to form •DMPO−OH as a stable radical.

$$V^{4+} + H_2O_2 \rightarrow V^{5+} + OH^- + {}^{\bullet}OH \quad (1)$$

$$DMPO + {}^{\bullet}OH \rightarrow {}^{\bullet}DMPO{-}OH \quad (2)$$

The EPR spectrum of the liquid phase, •DMPO−OH spin adducts, displays a characteristic 1:2:2:1 hyperfine splitting pattern ($a_N = a_{H\beta} = 14.96$ G). The intensities of •DMPO−OH in different catalysts are displayed in Figure 7. The EPR intensity is proportional to the concentration of active V^{4+} ions in the samples. The •DMPO−OH intensity is nearly zero for H_2O_2 in the presence of V−MCM-41 (vanadium oxides are on the framework of MCM-41; see Figure 7a), which is attributed to a very low concentration of active V^{4+} present after the calcination at 560 °C. The spectra in Figure 7b,c show the •DMPO−OH radical intensity for H_2O_2 in the presence of MCM41−NH_2−(VO)−H_2O and silica gel−NH_2−(VO)−H_2O samples. Prior to the EPR experiments, all these samples have been heated in air at 100 °C for 24 h. We observed the •DMPO−OH radical intensity in the silica gel−NH_2−(VO)−H_2O sample is greater than that of MCM41−NH_2−(VO)−H_2O sample, which may arise from the multiple $-O_3Si(CH_2)_3NH_2$ groups coordinating to one $(VO)^{2+}$ ion in the silica gel−NH_2−(VO)−H_2O sample. In other words, the multiple amino groups protect V^{4+} from oxidizing to V^{5+} under heating at 100 °C for 24 h.

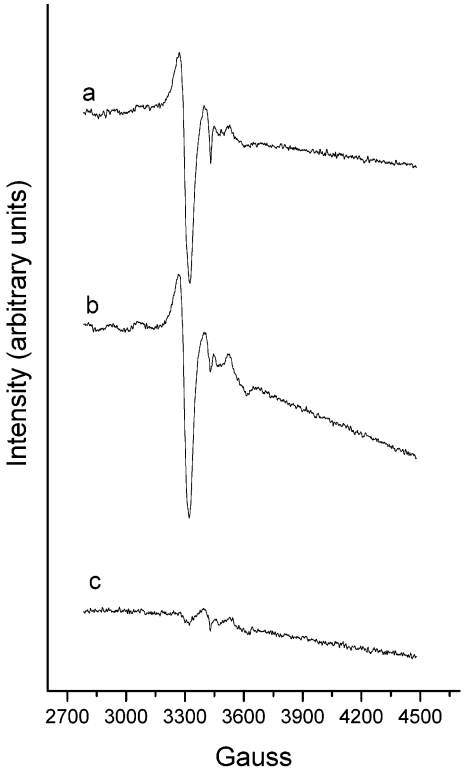

Figure 8. EPR spectra of the solids at 100 K after reaction with H_2O_2. The signal is assigned to dioxygen radical species: (a) V−MCM-41, (b) MCM41−NH_2−(VO)−EtOH, and (c) silica gel−NH_2−(VO)−EtOH. Note that the spectra show no trace of V^{4+} species, which leads us to assign the complex as V^{5+}−O−O•.

(b) Generation of Dioxygen Radicals. We allow the vanadium-containing catalysts to react with excess H_2O_2. Upon addition of H_2O_2, these catalysts immediately turn orange-red, typical for the formation of vanadium peroxide (see Scheme 3, complex **D**). The EPR spectra of the filtered solids at 100 K are shown in Figure 8. Scheme 3 shows that V^{4+} is oxidized to V^{5+} and releases •OH radicals in the presence of H_2O_2. The V^{4+} species can also react with two molecules of H_2O_2 to produce dioxygen centered radical species ($g = 2.005$) (complex **D**).[18,20] Since we did not observe any trace of V^{4+} in the EPR spectrum, we assign the vanadium peroxo complexes as V^{5+}−O−O•. On the basis of our EPR data and an earlier EPR study,[25] we can rule out the involvement of V^{4+}−O−O• in the hydroxylation or oxidation of hydrocarbons as proposed in a previous study.[26]

The spectra exhibit relatively higher concentrations of dioxygen radicals in both V−MCM-41 (Figure 8a) and MCM41−NH_2−(VO)−EtOH (Figure 8b) samples than in silica gel−NH_2−(VO)−EtOH sample (Figure 8c). The low dioxygen radical intensity in silica gel−NH_2−(VO)−EtOH sample may be attributed to the presence of strong ligand ($L = -O_3Si(CH_2)_3NH_2$) in the complex which is difficult to react with excess H_2O_2 to produce dioxygen radicals (see Scheme 3). These dioxygen radicals can promote the hydroxylation of hydrocarbons very effectively as shown below.

(c) Catalytic Hydroxylation of Benzene and the Leaching Amount of Vanadium in the Presence of H_2O_2 as Oxidant. The conversion and selectivity of these catalysts to the hydroxylation of benzene in the presence of H_2O_2 are given in Table 3. We note that MCM41−NH_2−(VO) has higher reactivity (47.2−58.6% of conversion) than silica gel−NH_2−(VO) samples (30.5−40.5% of conversion). We attribute the effect to the

TABLE 3: Total Conversion, Selectivity, and Metal Leaching of the Oxidation of Benzene in the Presence of H_2O_2 as an Oxidant[a,b]

	total conversion, %	selectivity of phenol, %	metal leaching, %
V−MCM-41	50.1	10.2	9.4
MCM41−NH_2−(VO)−EtOH[c]	51.6	15.9	2.7
MCM41−NH_2−(VO)−EtOH[d]	58.6	18.5	3.4
MCM41−NH_2−(VO)−H_2O[c]	47.2	11.2	1.2
MCM41−NH_2−(VO)−H_2O[d]	49.4	19.8	4.3
silica gel−NH_2−(VO)−EtOH[c]	30.5	28.6	13.3
silica gel−NH_2−(VO)−EtOH[d]	31.3	31.7	9.1
silica gel−NH_2−(VO)−H_2O[c]	36.2	26.4	8.6
silica gel−NH_2−(VO)−H_2O[d]	40.5	30.9	4.8

[a] Conditions of the catalytic reaction were as follows: 100 mg of catalyst, 10 mmol of benzene, 10 mmol of H_2O_2 (35%), 6 mL of CH_3CN, and reaction time 1 h. [b] Total conversion (%) = {([BA] − [BU])/[BA]} × 100; selectivity of phenol (%) = {[P]/([BA] − [BU])} × 100. [BA] is the amount of benzene added, [BU] is the amount of benzene unreacted, and [P] is the amount of phenol produced. [c] The catalyst was dried under vacuum. [d] The catalyst was dried in the oven at 100 °C for 24 h.

difference in structural distribution: the amount of complex **A** in MCM41−NH_2−(VO) is higher than that in silica gel−NH_2−(VO) sample. The good leaving group of EtOH or H_2O ligand in complex **A** enables MCM41−NH_2−(VO) sample to yield higher dioxygen radical concentration and higher catalytic activity. In general, the samples after heating have higher activity when H_2O_2 was used as an oxidant and this may be due to the oxidation of V^{4+} (complex **A**) to V^{5+} (complex **C**) in the heating process. The newly formed V^{5+} species can directly generate the V^{5+}−O−O$^{\bullet}$ radicals. These V^{5+}−O−O$^{\bullet}$ radicals are the active components for the hydroxylation of benzene.

Furthermore, we find the phenol selectivity (expressed in the percentage of phenol production as given in the footnote of Table 3) is higher in silica gel−NH_2−(VO) (26.4−31.7%) than in MCM41−NH_2−(VO) (11.2−19.8%) or V−MCM-41 (10.2%). From HPLC analysis, we find the products consist of phenol (the major component) and other higher oxidized compounds of phenol, such as catechol, hydroquinone, and 1,4-benzoquinone. The overoxidized products may arise from the fact that the phenol (polar molecule) has a higher reentry rate into the hydrophilic channels of MCM-41 than the nonpolar benzene. Once the phenol enters the reactive channels of MCM-41, it will undergo further oxidation or hydroxylation. Therefore, even though silica gel−NH_2−(VO) has lower overall catalytic reactivity, it provides better selectivity because less phenol can reenter silica gel−NH_2−(VO) and be overoxidized. We are striving to improve the characters of the channels so that we may enhance both the selectivity and reactivity.

Furthermore, we assess the stability of $(VO)^{2+}$ ions anchored on the functionalized MCM41−NH_2 surface. We employed ICP−AES to analyze the amount of vanadium metal leaching in the liquid mixture at the end of the catalytic reaction. We find the amount of metal leaching from the solids in MCM41−NH_2−(VO) is considerably lower (1.2−4.3%) than that in framework-substituted V−MCM-41 (9.4%). We attribute the effect to two factors: (1) the covalent bonding of the multiple amino group coordination to the vanadium oxide is stronger in MCM41−NH_2−(VO) or silica gel−NH_2−(VO), and (2) the calcinations at 560 °C to remove the template in the preparation of V−MCM-41 often seriously leach out the vanadium in the framework-substituted V−MCM-41. Therefore, our approaches to anchor vanadium on the modified surface have provided us with better stability in heterogeneous catalysis.

TABLE 4: Total Conversion, Selectivity, and Metal Leaching of the Oxidation of Benzene in the Presence of TBHP as an Oxidant[a]

	total conversion, %	selectivity of phenol, %	metal leaching, %
V−MCM-41	36.4	5.8	12.5
MCM41−NH_2−(VO)−EtOH[b]	46.5	6.3	6.9
MCM41−NH_2−(VO)−EtOH[c]	42.8	7.1	8.7
MCM41−NH_2−(VO)−H_2O[b]	30.2	6.4	0.8
MCM41−NH_2−(VO)−H_2O[c]	37.4	4.1	9.8
silica gel−NH_2−(VO)−EtOH[b]	21.4	12.5	1.1
silica gel−NH_2−(VO)−EtOH[c]	24.5	14.3	5.7
silica gel−NH_2−(VO)−H_2O[b]	22.9	10.7	1.2
silica gel−NH_2−(VO)−H_2O[c]	26.2	13.2	8.1

[a] Conditions of the catalytic reaction were as follows: 100 mg of catalyst, 10 mmol of benzene, 10 mmol of TBHP (70%), 6 mL of CH_3CN, and reaction time 6 h. [b] The catalyst was dried under vacuum. [c] The catalyst was dried in the oven at 100 °C for 24 h.

(d) Catalytic Hydroxylation of Benzene and the Leaching Amount of Vanadium in the Presence of TBHP as an Oxidant. Using TBHP in place of H_2O_2 as an oxidant (Table 4), we also find that MCM41−NH_2−(VO) has a higher conversion rate (30.2−46.5%) than silica gel−NH_2−(VO) (21.4−26.2%). In addition, the conversion of MCM41−NH_2−(VO)−EtOH (46.5%) is higher than that of MCM41−NH_2−(VO)−H_2O sample (30.2%). The higher reactivity of MCM41−NH_2−(VO)−EtOH sample may come from the weaker binding strength of the EtOH ligand in complex **A** which is easily replaced by H_2O_2 to yield V^{5+}−O−O$^{\bullet}$ radicals.

In the determination of the amount of metal leaching, we also find the extraframework vanadium oxide catalyst has lower metal leaching (0.8−9.8%) than V−MCM-41 (12.5%). In addition, the samples dried in the oven at 100 °C for 24 h have more metal leaching than those under vacuum. It may arise from the formation of highly coordinated complex (i.e., octahedral or square pyramidal) in the heating process, and these complexes are unstable in the presence of TBHP. Note that the experimental conditions for applying H_2O_2 and TBHP as oxidants are different in their concentrations and reaction times. Therefore, it is inappropriate to compare the results between these two data sets.

Conclusions

We have demonstrated by proper surface functionalization of MCM-41 solids with amino groups that the high content of active vanadyl ions $(VO)^{2+}$ can be immobilized on the surface of mesoporous solids at room temperature as shown in elemental analysis and leaching studies. The method of preparation differs from the framework-substituted V−MCM-41 solids, which were prepared by calcinations at 540 °C for 8 h. Our studies of the catalytic reactivity in the generation of $^{\bullet}$OH and reactive dioxygen radicals, and in the hydroxylation of benzene, further demonstrate the utilities of this new class of functionalized catalyst: they are better than the framework-substituted V−MCM-41 solids in conversion rate, product selectivity, and metal leaching. Our choice of the simple functional group APTS is good for the control of surface ligand density since it has been well-studied previously.[12,13] One may further employ other complex ligands which have been developed previously,[27] so that we may further exploit the power of homogeneous catalysis along the same approaches.

In this study, we have further demonstrated that functionalized mesoporous materials possess the advantages of the isolation of the catalytic site where well-defined molecular species can

be placed and controlled. The control of the density of functionalization leads to the control of availability of mobile ligands, which affects the overall chemical reactivity. One may envision that several well-defined reactive sites can be simultaneously designed to locate in a neighboring region within the nanopores to gain better control of the complex reaction system. These mesoporous materials with 2−10 nm pores provide the means and opportunity to probe many complex chemical reactions of bulky substrates in nanoreactors as we recently demonstrated.[28] Reactions involving physically constrained molecules could lead to new fundamental understanding about the use of local environment to control chemical reactions.

Acknowledgment. This work was supported partially by grants to C.-Y.M. from the Ministry of Education through Academy Excellent program and NSC International program (NSC 90-2113-M-002-057). T.-S.L. acknowledges partial support by a grant from NSF-International Program (NSF No. 0115082) and a PRF grant administered by the American Chemical Society (No. 36970).

References and Notes

(1) Kresge, C. T.; Leonowicz, M. E.; Roth, W. J.; Vartuli, J. C.; Beck, J. S. *Nature* **1992**, *359*, 710.
(2) Brunel, D. *Microporous Mesoporous Mater.* **1999**, *27*, 329.
(3) Corma, A.; Kumar, D. *Stud. Surf. Sci. Catal.* **1998**, *117*, 201.
(4) Scott, B. J.; Wirnsberger, G.; Stucky, G. D. *Chem. Mater.* **2001**, *13*, 3140.
(5) Brieler, F. J.; Froba, M.; Chen, L. M.; Klar, P. J.; Heimbrodt, W.; Von Nidda, H. A. K.; Loidl, A. *Chem. Eur. J.* **2002**, *8*, 185.
(6) Davis, M. E. *Nature* **2002**, *417*, 813.
(7) Lin, H. P.; Mou, C. Y. *Acc. Chem. Res.* **2002**, *35*, 927.
(8) Wong, S. T.; Lin, H. P.; Mou, C. Y. *Appl. Catal. A* **2000**, *198*, 103.
(9) Lee, C. W.; Lee, W. J.; Park, Y. K.; Park, S. E. *Catal. Today* **2000**, *61*, 137.
(10) Chen, Y. W.; Lu, Y. H. *Ind. Eng. Chem. Res.* **1999**, *38*, 1893.
(11) De Vos, D. E.; Sels, B. F.; Jacobs, P. A. *Adv. Catal.* **2001**, *46*, 1.
(12) Carvalho, W. A.; Wallau, M.; Schuchardt, U. *J. Mol. Catal. A* **1999**, *144*, 91.
(13) Evans, J.; Zaki, A. B.; El-Sheikh, M. Y.; El-Safty, S. A. *J. Phys. Chem. B* **2000**, *104*, 10271.
(14) Weissermel, K.; Arpe, H. J. *Industrial Organic Chemistry*, 3rd revised ed.; VCH Publishers: New York, 1997; p 354; translated by C. R. Lindely.
(15) Lin, H. P.; Cheng, Y. R.; Lin, C. R.; Li, F. Y.; Chen, C. L.; Wong, S. T.; Cheng, S. F.; Liu, S. B.; Wan, B. Z.; Mou, C. Y.; Tang, C. Y.; Lin, C. Y. *J. Chin. Chem. Soc.* **1999**, *46*, 495.
(16) Beck, J. S.; Vartuli, J. C.; Roth, W. J.; Leonowicz, M. E.; Kresge, C. T.; Schmitt, K. D.; Chu, C. T. W.; Olson, D. H.; Sheppard, E. W.; Mccullen, S. B.; Higgins, J. B.; Schlenker, J. L. *J. Am. Chem. Soc.* **1992**, *114*, 10834.
(17) Mathieu, M.; Van Der Voort, P.; Weckhuysen, B. M.; Rao, R. R.; Catana, G.; Schoonheydt, R. A.; Vansant, E. F. *J. Phys. Chem. B* **2001**, *105*, 3393.
(18) Chao, K. J.; Wu, C. N.; Chang, H.; Lee, L. J.; Hu, S. F. *J. Phys. Chem. B* **1997**, *101*, 6341.
(19) Chatterjee, M.; Iwasaki, T.; Hayashi, H.; Onodera, Y.; Ebina, T.; Nagase, T. *Chem. Mater.* **1999**, *11*, 1368.
(20) Neumann, R.; Levin-Elad, M. *Appl. Catal. A* **1995**, *122*, 85.
(21) Luan, Z. H.; Xu, J.; He, H. Y.; Klinowski, J.; Kevan, L. *J. Phys. Chem.* **1996**, *100*, 19595.
(22) Prakash, A. M.; Kevan, L. *J. Phys. Chem. B* **1999**, *103*, 2214.
(23) Prakash, A. M.; Kevan, L. *J. Phys. Chem. B* **2000**, *104*, 6860.
(24) Bogomolova, L. D.; Jachkin, V. A.; Krasil'nikova, N. A. *J. Non-Cryst. Solids* **1998**, *241*, 13.
(25) Brooks, H. B.; Sicilio, F. *Inorg. Chem.* **1971**, *10*, 2530.
(26) Mimoun, H.; Saussine, L.; Daire, E.; Postel, M.; Fischer, J.; Weiss, R. *J. Am. Chem. Soc.* **1983**, *105*, 3101.
(27) Knops-Gerrits, P. P.; Trujillo, C. A.; Zhan, B. Z.; Li, X. Y.; Jacobs, P. A. *Top. Catal.* **1996**, *3*, 437.
(28) Lee, C. H.; Lin, T. S.; Mou, C. Y. *Phys. Chem. Chem. Phys.* **2002**, *4*, 3106.